Available online at www.sciencedirect.com
ScienceDirect
Nuclear Physics B Proceedings Supplement 00 (2014) 1–7
Nuclear Physics B Proceedings Supplement

Measurement of the electroweak production cross section of same-sign $W^{\pm}W^{\pm}$ bosons associated with dijets with the ATLAS detector

Christian Gumpert*

Institute of Nuclear and Particle Physics, Technical University Dresden, Zellescher Weg 19, 01069 Dresden, Germany

Abstract

A measurement of the production cross section for two same-sign $W^{\pm}$ bosons in association with dijets was performed using 20.3 fb^{-1} of proton-proton collision data collected at $\sqrt{s} = 8$ GeV with the ATLAS detector. The background-only hypothesis was rejected at the 4.5σ confidence level and the measured fiducial cross section is in agreement with the Standard Model prediction. Evidence for the electroweak component of this process was observed at the 3.6σ level and a measurement of the fiducial cross section for the electroweak production of the $W^{\pm}W^{\pm}jj$ final state was reported. The electroweak component contains contributions from vector boson scattering diagrams. Thus, the fiducial cross section measurement was used to derive constraints on exotic contributions to the quartic $WWWW$ gauge boson vertex. In these proceedings, a brief description of the analysis is presented.

Keywords: W boson, electroweak, Standard Model, anomalous couplings

1. Introduction

Scattering processes of two heavy vector bosons (VBS) are a crucial probe to study the nature of electroweak symmetry breaking. In the absence of a Standard Model (SM) Higgs boson, the scattering cross section for longitudinally polarised vector bosons raises with increasing $\sqrt{s}$ and violates unitarity eventually. Given the recent discovery [1, 2] of a scalar boson with a mass of 125 GeV at the Large Hadron Collider (LHC) [3], the question remains whether this is *the* SM Higgs boson [4–9]. Hitherto, the particle properties measured are in agreement with the SM prediction [10–14]. However, there is not yet any experimental data available on the cross sections for the scattering of heavy vector bosons. Those measurements are essential to decide whether the particle discovered regularises the VBS amplitudes completely as predicted by the SM. Extensions of the SM electroweak sector suggest alternative electroweak symmetry breaking mechanisms involving additional resonances [15, 16]. Therefore, the study of VBS processes is a key to ultimately answer the question about the nature of the electroweak symmetry breaking mechanism.

At the LHC, VBS processes occur due to interactions between two vector bosons which are radiated off the incoming quarks. Example Feynman diagrams for the process $pp \to \ell^{\pm}\nu\ell'^{\pm}\nu' jj$ are shown in Figure 1.

The contributing diagrams at lowest order perturbation theory can be classified into two disjoint sets[1]:

1. Diagrams only containing electroweak vertices are of the order $O\left(g^6\right)$ and will be referred to as the *electroweak* (EWK) component.
2. Diagrams containing both electroweak and strong vertices are of the order $O\left(g^4 g_s^2\right)$ and will be referred to as the *strong* (QCD) component.

*On behalf of the ATLAS Collaboration

[1] In the following, g denotes the coupling constant for the $SU(2)_L$ gauge symmetry of the Standard Model of Particle Physics while g_s is the coupling constant for the $SU(3)_C$ gauge symmetry.

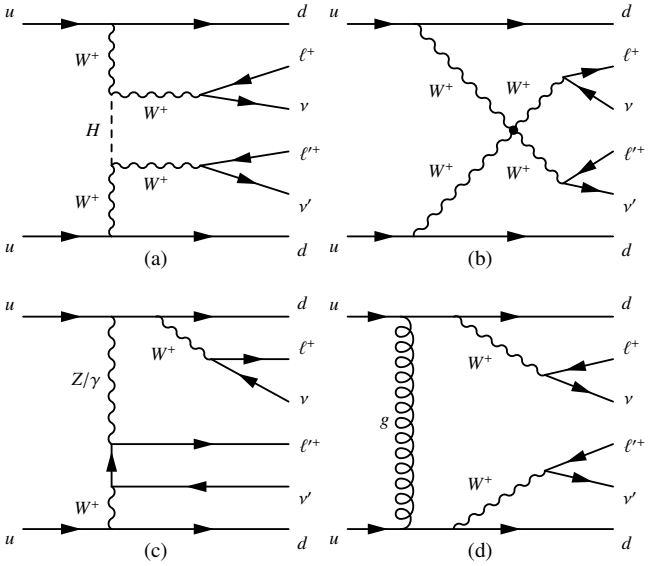

Figure 1: Example Feynman diagrams for the process $uu \to \ell^+\nu\ell'^+\nu' dd$: (a) and (b) VBS diagrams; (c) non-resonant contribution; (d) strong mediated production.

Evidently, the EWK component contains the VBS diagrams and, hence, is sensitive to the electroweak symmetry breaking mechanism which makes this process especially interesting. Investigating the scattering of same-sign $W^\pm$ bosons is particularly motivated by the absence of gg initiated QCD processes for this final state, that significantly improves the cross section ratio $\sigma^{\text{EWK}}_{\text{fid}}/\sigma^{\text{QCD}}_{\text{fid}}$ in a VBS enhanced phase space. This unique feature greatly facilitates the extraction of the EWK component of the $pp \to \ell^\pm\nu\ell'^\pm\nu' jj$ process (hereinafter referred to as $W^\pm W^\pm jj$)[2].

However, the QCD component constitutes a significant contribution in an inclusive phase space. As none of the two categories had been observed before, this analysis focused on a measurement of the inclusive production cross section of the process $W^\pm W^\pm jj$ in a fiducial phase space. Furthermore, another more restricted phase space was used to extract the fiducial cross section of the EWK component and to constrain possible exotic contributions to the $WWWW$ vertex.

In these proceedings, a brief description of the analysis is presented. The reader is referred to the journal publication [17] for more details.

[2]The reader is reminded that this shorthand notation also contains non-resonant contributions including e.g. the exchange of virtual $W^\pm$ bosons.

2. Theory

Theoretical predictions were calculated in two fiducial regions which mimic the event selection criteria applied on detector level. The *inclusive region* is defined at particle level as follows. Exactly two prompt charged leptons, excluding τ leptons and leptons originating from τ decays, are required with same electric charge, transverse momentum $p_{\text{T}} > 25$ GeV and $|\eta| < 2.5$. In order to reduce the dependence on the modelling of QED radiation, lepton four-momenta include the contributions from photons within a cone of $\Delta R \leq 0.1$ around the lepton. The dilepton invariant mass must exceed 20 GeV and the angular separation of the two leptons is required to be $\Delta R_{\ell\ell} = \sqrt{(\Delta\phi)^2 + (\Delta\eta)^2} > 0.3$. The missing transverse energy reconstructed from all neutrinos in the final state must be greater than 40 GeV. Jets are reconstructed using the anti-k_t algorithm [18] with a radius parameter of $R = 0.4$. They are required to have $p_{\text{T}} > 30$ GeV and $|\eta| < 4.5$. Events are selected if there are at least two jets in the event. Furthermore, the two leptons have to be well separated from all selected jets in the event by imposing $\min_{\ell,j} \Delta R_{\ell j} > 0.3$. The two highest p_{T} jets are referred to as *tagging jets* and they must have an invariant dijet mass $m_{jj} > 500$ GeV. This phase space is used to measure the production cross section for the process $W^\pm W^\pm jj$ treating both the EWK and the QCD contribution as well as their interference as signal.

The second fiducial volume is designed to enhance the contribution from the EWK component by requiring in addition to the aforementioned selection criteria that the separation of the two tagging jets in rapidity satisfies $|\Delta y_{jj}| > 2.4$. This phase space, referred to as *VBS region*, is used to extract the EWK component while considering the QCD contribution as background.

The Powheg-Box framework [19–23], with the CT10 parton distribution function (PDF) [24], interfaced to Pythia8 [25, 26] for parton showering, hadronisation, QED final state radiation and underlying event modelling using the ATLAS AU2 tune [27], was used to calculate fiducial cross sections for the EWK and QCD components of the process $W^\pm W^\pm jj$ at next-to-leading order (NLO) in QCD using a dynamic scale of $\mu_F = \mu_R = \sum_{i=1}^{2} \left(p_{\text{T},j_i} + 0.5 \sqrt{m_W^2 + p_{\text{T},W_i}^2} \right)$. Uncertainties on the predicted fiducial cross sections include the statistical error from the Monte Carlo (MC) integration, 68% confidence level PDF uncertainties as well as effects from the independent variations of the factorisation and renormalisation scales by a factor of two. Generator uncertainties were estimated by comparing predictions from Powheg-Box and VBFNLO [28, 29].

The effect of the parton shower and hadronisation modelling uncertainties were derived by replacing Pythia8 by Herwig++/Jimmy [30, 31]. The interference between the EWK and QCD component were estimated at leading order (LO) QCD with Sherpa [32] using a fixed scale of $\mu_F = \mu_R = 2m_W$. It was found that the interference contribution amounts to $(10.6 \pm 5.4)\%$ and $(6.5 \pm 3.5)\%$ of the total fiducial cross section for the $W^\pm W^\pm jj$ process in the inclusive and VBS region, respectively. The uncertainties include effects from the limited statistical precision of the MC integration as well as a conservative relative uncertainty on the interference contribution of 50% to account for the different scale choice and the lower formal accuracy of the calculation.

In the inclusive region, the total predicted cross section at NLO QCD is 1.52 ± 0.11 fb which includes an interference contribution of 0.16 ± 0.08 fb. The sum of the EWK and interference contribution in the VBS region is 0.95 ± 0.06 fb. The parton shower and generator uncertainties are dominant for the EWK production while the scale uncertainties are dominant for the strong production.

3. Data selection and analysis methodology

The measurement was performed using proton-proton collision data at $\sqrt{s} = 8$ GeV recorded by the ATLAS experiment. The ATLAS detector is described in detail elsewhere [33].

Events for this analysis were selected by a combination of single-electron and single-muon triggers with the lowest p_{T} threshold being 24 GeV. After having applied data quality criteria, the data set corresponded to an integrated luminosity of 20.3 fb^{-1}.

Electron candidates were required to fall inside the kinematic acceptance of $p_{\mathrm{T}} > 25$ GeV and $|\eta| < 2.47$. The transition region at $1.37 < |\eta| < 1.52$ between the barrel and endcap calorimeters was excluded. Additionally, electron candidates must pass the tight quality selection criteria, as described in [34], which were reoptimised for data taking in 2012. Muon candidates [35] were required to pass $p_{\mathrm{T}} > 25$ GeV and $|\eta| < 2.5$. The muon charge must be measured consistently in the inner detector and in the muon spectrometer. Furthermore, stringent requirements on the longitudinal and transverse impact parameters of the lepton candidates were applied together with tight cuts on calorimeter- and track-based isolation variables in order to reduce background contributions from non-prompt lepton production. Jet candidates were reconstructed from energy deposits in the calorimeters, clustered with the anti-k_t algorithm with radius parameter $R = 0.4$ and calibrated as described in [36]. Only candidates with $p_{\mathrm{T}} > 30$ GeV and $|\eta| < 4.5$ were considered. In order to suppress background from multiple simultaneous interactions, jets with $p_{\mathrm{T}} < 50$ GeV and $|\eta| < 2.4$ were only accepted if the tracks associated to the jet and originating from the primary vertex constitute at least 50% of the jet's total transverse momentum. Jets containing b-hadrons were identified by an algorithm which combines information from secondary vertex reconstruction and the significance of track impact parameters. The chosen working point for the b-tagging algorithm was 70% efficient on real b-jets [37]. The missing transverse energy, $E_{\mathrm{T}}^{\mathrm{miss}}$, was calculated from the energy collected in the calorimeters and the reconstructed muons tracks [38].

Candidate $W^\pm W^\pm jj$ events were required to have exactly two light leptons ($= e, \mu$) of same electric charge with a dilepton invariant mass of $m_{\ell\ell} > 20$ GeV, at least two jets and missing transverse energy of $E_{\mathrm{T}}^{\mathrm{miss}} > 40$ GeV. Furthermore, events with additional lepton candidates passing a looser object selection with lowered p_{T} thresholds of 6 GeV/7 GeV for muons/electrons were rejected to suppress background events from $W^\pm Z/\gamma^* jj$ processes. Also, events with at least one jet labeled as b-jet were discarded to reduce the contamination from $t\bar{t} + W/Z$ events. Events in the $e^\pm e^\pm$ final state were removed if the dielectron mass was within a window of 10 GeV around the Z boson mass to reduce the background from Z + jets events due to electron charge misidentification. In order to further reduce the background, events in the inclusive region were required to have a tagging jet invariant mass of $m_{jj} > 500$ GeV. The VBS signal region was defined by requiring in addition the separation in rapidity of the two tagging jets to be $|\Delta y_{jj}| > 2.4$.

4. Background modelling

The signal processes and several background processes were modelled using MC simulation. The signal events were simulated using Sherpa with up to three jets from the matrix element matched to the parton shower model. These samples were normalised in the respective fiducial regions to the aforementioned fiducial cross sections. Generated events were processed with the full simulation of the ATLAS detector [39] based on Geant4 [40] and reconstructed using the standard ATLAS software.

Several SM processes enter the $W^\pm W^\pm jj$ signal regions as irreducible physics background or due to instrumental/reconstruction effects. The background contributions were classified into three categories:

1. Prompt leptons: SM processes with three or more leptons populate the signal regions due to one or more leptons being outside the kinematic acceptance or failing the lepton object selection criteria.
2. Conversions: This background category only affects the channels with an electron in the final state where the electron may originate from a converted photon. Effects due to the mismeasurement of the electron charge are included herein.
3. Other non-prompt leptons: Events with at least one lepton candidate coming from hadron decays in jets or with jets being misclassified as leptons are contained in this category.
4. Double parton scattering contributions were examined using simulation and found to be negligible after the $m_{jj} > 500$ GeV requirement.

The $W^{\pm}Z/\gamma^{*}jj$ process constituted about 90% of the prompt lepton background where abouth one fifth of the expected $W^{\pm}Z/\gamma^{*}jj$ events came from EWK production. This background was modelled using Sherpa and normalised to NLO QCD cross sections in the fiducial regions calculated with VBFNLO [41, 42]. The contained tZj component in this sample was normalised to the LO QCD Sherpa prediction. The remaining fraction of the prompt lepton background arose from ZZ + jets processes (modelled with Sherpa) and $t\bar{t} + W/Z$ events (simulated with MadGraph [43]).

Events from the $pp \to W^{\pm}\gamma jj$ process where the photon converts to an electron-positron pair in the detector was included in the conversion background. It was generated using Alpgen [44] + Herwig++/Jimmy. The electroweak component of this process includes $W^{\pm}\gamma$ scattering and was simulated with Sherpa. Of equal importance for the conversion background are $Z/\gamma^{*} \to e^{+}e^{-}$ events and $t\bar{t}$ production with leptonic decays of the $W^{\pm}$ bosons. The case of hard bremsstrahlung emitted by an electron subsequently followed by an asymmetric photon conversion into an electron-positron pair can lead to a confusion in the measurement of the electric charge of the reconstructed electron. Using a likelihood approach, the charge misidentification rate for electrons was measured in data using $Z/\gamma^{*} \to e^{+}e^{-}$ events while it was found to be negligible for muons. It was observed that the strict requirements on the transverse impact parameter of the electron candidates of $d_0/\sigma(d_0) < 3$ significantly reduced the charge misidentification rate which varies between 0.02% and 2% depending on the η of the electron candidate. This background component was estimated by defining a control sample in data using the same event selection criteria except for the lepton charge correlation which changed to demand exactly two oppositely charged lepton candidates. This control sample was scaled by the electron charge misidentification rate applied as event weight to obtain the background estimate in the signal region. Corrections to the energy of the electron candidate, which were derived from simulation, were applied to account for the energy loss experienced by the initial electron during the conversion process. Dominant uncertainties arose from the limited data statistics in the control sample and a possible bias of the method studied in simulation.

The contribution from the "other non-prompt leptons" category (containing events from $W^{\pm}$ + jets, $t\bar{t}$, single top or multijet processes) was estimated using a data-driven approach. A control sample enriched in events with at least one lepton coming from hadron decays or misidentification of jets was constructed by requiring events with exactly one lepton candidate passing the nominal object selection criteria and a second lepton candidate passing a modified object selection. The modified object criteria asked for lepton candidates which were not isolated or of loose quality. They were designed to be orthogonal to the nominal lepton object definition. These events were weighted by a "fake rate" to obtain an estimate of this background component in the signal regions. The "fake rate" was defined as the ratio of the probability for a non-prompt lepton to pass the nominal object selection divided by the efficiency to pass the modified ("fake"-enriched) lepton selection. A dijet control sample in data was used to measure the "fake rate" for non-prompt leptons as a function of the p_{T} of the lepton candidate. Contamination from prompt lepton production in this dijet control sample was corrected using simulation which introduced the dominant source of uncertainty on this background estimate.

Correction factors were applied to simulation in order to account for differences observed in object reconstruction/identification efficiencies and modelling of pile-up with respect to data. Furthermore, the simulation was tuned to reproduce the lepton and jet energy scale and resolution as measured in data. Background estimates based on MC simulation were scaled to the most precise theoretical predictions available. Their uncertainties include effects from scale variations and PDF uncertainties as well as uncertainties from parton shower and hadronisation model. Experimental uncertainties were derived from uncertainties on the correction factors, the $E_{\mathrm{T}}^{\mathrm{miss}}$ modelling and by varying the lepton energy/momentum scale and resolution parameters. The total systematic uncertainty on the background prediction in the signal regions was about 20%. It was dominated by the uncertainty on the jet energy scale ($\approx 11 - 15\%$) followed by the accuracy of the the-

control region		trilepton	≤ 1 jet	b-tag	low m_{jj}
$e^{\pm}e^{\pm}$	exp.	36 ± 6	278 ± 28	40 ± 6	76 ± 9
	data	40	288	46	78
$e^{\pm}\mu^{\pm}$	exp.	110 ± 18	288 ± 42	75 ± 13	127 ± 16
	data	104	328	82	120
$\mu^{\pm}\mu^{\pm}$	exp.	60 ± 10	88 ± 14	25 ± 7	40 ± 6
	data	48	101	36	30

Table 1: Summary of expected event yields with total uncertainty and number of events observed in data split up by channel for various control regions.

ory predictions ($\approx 4 - 11\%$).

The validity and robustness of the background estimation techniques were carefully checked in several control regions, each of which designed to target specific background contributions.

- The *trilepton* control region, defined by inverting the third lepton veto and dropping the requirements on m_{jj} and $|\Delta y_{jj}|$, was used to test the modelling of the m_{jj} and $|\Delta y_{jj}|$ distributions of the $W^{\pm}Z/\gamma^{*}jj$ background.
- Events with at most one jet form the ≤ 1 *jet* control sample. In this region, the description of the conversion background was validated in the $e^{\pm}e^{\pm}$ final state, while the $\mu^{\pm}\mu^{\pm}$ was dominated by background from prompt leptons, and the $e^{\pm}\mu^{\pm}$ contained a mixture of both.
- The *b-tag* control region, defined by inverting the b-jet veto, was used to verify the background modelling for non-prompt leptons from $t\bar{t}$ processes.
- The *low* m_{jj} control region, defined by inverting the $m_{jj} > 500$ GeV selection criterion, tests the combined background model.

A comparison of the predicted and observed event yields for the various control regions is given in Table 1. Figure 2 illustrates the good description of important variables by the background model.

5. Cross section measurement

The number of expected and observed events in the two regions, split up by channel, is given in Table 2. Figure 3 shows the separation in rapidity of the two tagging jets in the inclusive region. The calculation of significances and the extraction of fiducial cross sections was based on the number of events observed per channel. In both regions, an excess over the background-only hypothesis was observed corresponding to a significance of $4.5\sigma/3.6\sigma$ in the inclusive/VBS region. The excess in the inclusive region was interpreted as $W^{\pm}W^{\pm}jj$ production and its fiducial cross section was extracted using a likelihood approach. Correcting for the efficiency of detector level effects (e.g., reconstruction and identification efficiencies) as well as for migration into and out of the fiducial region, the combined fiducial cross section for $W^{\pm}W^{\pm}jj$ production in the inclusive region was measured to be $2.1 \pm 0.5(\text{stat}) \pm 0.3(\text{syst})$ fb. The excess in the VBS region was interpreted as EWK $W^{\pm}W^{\pm}jj$ production and its extracted fiducial cross section was $1.3 \pm 0.4(\text{stat}) \pm 0.2(\text{syst})$ fb, including the interference contribution. The measured values are in agreement with the respective SM predictions of 1.52 ± 0.11 fb and 0.95 ± 0.06 fb.

6. Constraints on anomalous gauge couplings

The measured fiducial cross section for the $W^{\pm}W^{\pm}jj$ EWK production in the VBS region allowed to derive first direct limits on anomalous quartic gauge couplings (aQGC) affecting the $WWWW$ vertex. For this analysis, an implementation of an effective field theory approach [45] in Whizard [46, 47] was used to express additional contributions to EWK fiducial cross section in terms of anomalous coupling parameters α_4 and α_5. Fiducial cross sections in the VBS region as a function of α_4 and α_5 were determined by interfacing events generated with Whizard at LO QCD, using the CTEQ6L1 PDF set [48] and applying the K-matrix unitarisation scheme [45], to Pythia8 for parton shower and underlying event modelling. A constant k-factor was applied to match the cross section predicted by Powheg-Box + Pythia8 at the SM point corresponding to $\alpha_4 = \alpha_5 = 0$. Points in the $\alpha_4 \times \alpha_5$ plane were excluded at 95% confidence level if the corresponding predicted fiducial cross section was incompatible with the measured value at the 95% confidence level. Hereby, the change in signal reconstruction efficiency as function of the aQGC values, which had been estimated from fully simulated Whizard samples, was taken into account. The derived two-dimensional confidence intervals are shown in Figure 4. Due to an upward fluctuation in data, the exclusion contours observed are less stringent than the expected limits.

References

[1] ATLAS Collaboration, Phys.Lett.B 716 (2012) 1.
[2] CMS Collaboration, Phys.Lett.B 716 (2012) 30.

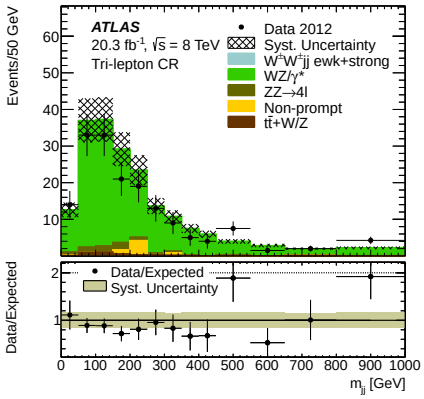

(a) Tagging jets invariant mass in the trilepton region.

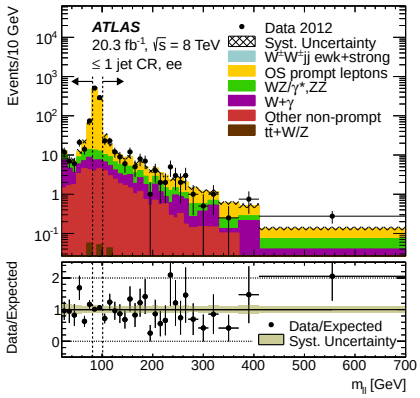

(b) Dielectron invariant mass in the $e^{\pm}e^{\pm}$ channel in the ≤ 1 jet region.

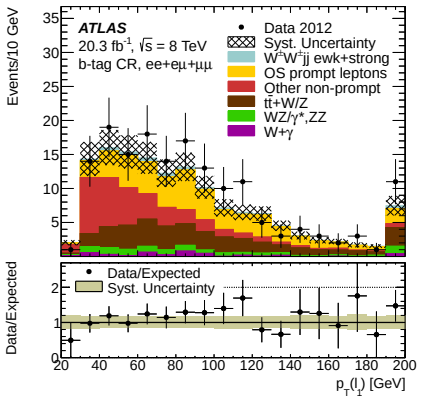

(c) Transverse momentum of the leading lepton in the b-tag region.

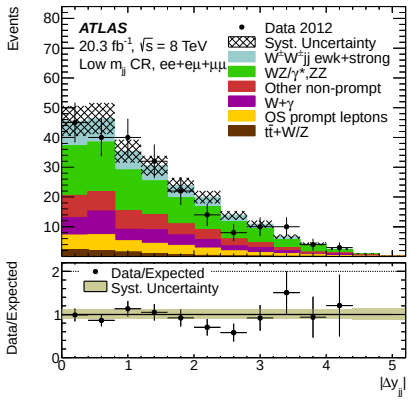

(d) Separation in rapidity of the tagging jets in the low m_{jj} region.

Figure 2: Validation plots for the background modelling of different variables in the various control regions. The stacked histograms represent the expectation estimated as described in the text while the black points show the distribution observed in data. The hatched band indicates the total uncertainty on the prediction. The ratio of the data distribution to the expected distribution is shown in the bottom panels.

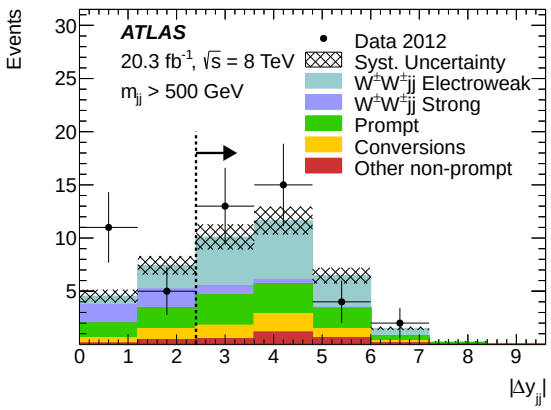

Figure 3: Separation in rapidity of the two tagging jets in the inclusive region. The dashed line with the arrow indicates the VBS region.

[3] L. Evans, P. Bryant (editors), LHC Machine, JINST 3 (2008) S08001.
[4] F. Englert, R. Brout, Phys. Rev. Lett. 13 (1964) 321.
[5] P. W. Higgs, Phys. Lett. 12 (1964) 132.
[6] P. W. Higgs, Phys. Rev. Lett. 13 (1964) 508.
[7] G. Guralnik, C. Hagen, T. Kibble, Phys. Rev. Lett. 13 (1964) 585.
[8] P. W. Higgs, Phys. Rev. 145 (1966) 1156.
[9] T. Kibble, Phys. Rev. 155 (1967) 1554.
[10] ATLAS Collaboration, Phys.Lett. B726 (2013) 120–144.
[11] CMS Collaboration, CMS-PAS-HIG-14-012, `https://cds.cern.ch/record/1728250`.
[12] CMS Collaboration, Phys.Rev.Lett. 110 (2013) 081803.
[13] ATLAS Collaboration, ATLAS-CONF-2014-009, `https://cds.cern.ch/record/1670012`.
[14] CMS Collaboration, CMS-PAS-HIG-14-009, `https://cds.cern.ch/record/1728249`.
[15] D. Espriu, B. Yencho, Phys. Rev. D 87 (2013) 055017.
[16] J. Chang, K. Cheung, et al., Phys. Rev. D 87 (2013) 093005.
[17] ATLAS Collaboration, Phys. Rev. Lett. 113 (2014) 141803.

	inclusive region			VBS region		
	$e^\pm e^\pm$	$e^\pm \mu^\pm$	$\mu^\pm \mu^\pm$	$e^\pm e^\pm$	$e^\pm \mu^\pm$	$\mu^\pm \mu^\pm$
Prompt	3.0 ± 0.7	6.1 ± 1.3	2.6 ± 0.6	2.2 ± 0.5	4.2 ± 1.0	1.9 ± 0.5
Conversions	3.2 ± 0.7	2.4 ± 0.8	–	2.1 ± 0.5	1.9 ± 0.7	–
Other non-prompt	0.61 ± 0.30	1.9 ± 0.8	0.41 ± 0.22	0.50 ± 0.26	1.5 ± 0.6	0.34 ± 0.19
$W^\pm W^\pm jj$ QCD	0.89 ± 0.15	2.5 ± 0.4	1.42 ± 0.23	0.25 ± 0.06	0.71 ± 0.14	0.38 ± 0.08
$W^\pm W^\pm jj$ EWK	3.07 ± 0.30	9.0 ± 0.8	4.9 ± 0.5	2.55 ± 0.25	7.3 ± 0.6	4.0 ± 0.4
Total background	6.8 ± 1.2	10.3 ± 2.0	3.0 ± 0.6	5.0 ± 0.9	8.3 ± 1.6	2.6 ± 0.5
Total expected	10.7 ± 1.4	21.7 ± 2.6	9.3 ± 1.0	7.6 ± 1.0	15.6 ± 2.0	6.6 ± 0.8
Data	12	26	12	6	18	10

Table 2: Summary of expected event yields from various background processes with their total uncertainty in the two signal regions, split up by channel. The number of events observed in data is also given for each channel. The $W^\pm W^\pm jj$ EWK component was scaled to include the contribution from interference. In the inclusive region, the sum of EWK and QCD $W^\pm W^\pm jj$ were considered as signal while in the VBS region, $W^\pm W^\pm jj$ QCD was treated as background.

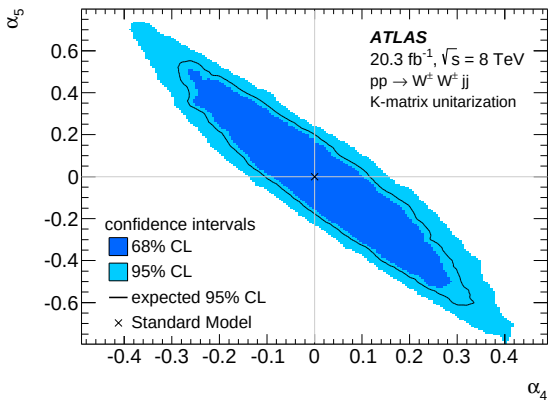

Figure 4: Two-dimensional confidence intervals in the $\alpha_4 \times \alpha_5$-plane. The filled areas indicate the observed confidence intervals while the black line represents the expected 95% exclusion contour.

[18] M. Cacciari, G. P. Salam, G. Soyez, JHEP 0804 (2008) 063.
[19] P. Nason, JHEP 0411 (2004) 040.
[20] S. Frixione, P. Nason, C. Oleari, JHEP 0711 (2007) 070.
[21] S. Alioli, P. Nason, C. Oleari, E. Re, JHEP 1006 (2010) 043.
[22] B. Jaeger, G. Zanderighi, JHEP 1111 (2011) 055.
[23] T. Melia, P. Nason, R. Rontsch, G. Zanderighi, Eur.Phys.J. C71 (2011) 1670.
[24] H.-L. Lai, M. Guzzi, J. Huston, Z. Li, P. M. Nadolsky, et al., Phys.Rev. D82 (2010) 074024.
[25] T. Sjostrand, S. Mrenna, P. Z. Skands, JHEP 0605 (2006) 026.
[26] T. Sjostrand, S. Mrenna, P. Z. Skands, Comput.Phys.Commun. 178 (2008) 852–867.
[27] ATLAS Collaboration, ATL-PHYS-PUB-2012-003, `https://cds.cern.ch/record/1474107`.
[28] K. Arnold, M. Bahr, G. Bozzi, F. Campanario, C. Englert, et al., Comput.Phys.Commun. 180 (2009) 1661–1670.
[29] B. Jaeger, C. Oleari, D. Zeppenfeld, Phys.Rev. D80 (2009) 034022.
[30] M. Bahr, S. Gieseke, M. Gigg, D. Grellscheid, K. Hamilton, et al., Eur.Phys.J. C58 (2008) 639–707.
[31] J. Butterworth, J. R. Forshaw, M. Seymour, Z.Phys. C72 (1996) 637–646.
[32] T. Gleisberg, S. Hoeche, F. Krauss, M. Schonherr, et al., JHEP 0902 (2009) 007.
[33] ATLAS Collaboration, JINST 3 (2008) S08003.
[34] ATLAS Collaboration, Eur.Phys.J. C72 (2012) 1909.
[35] ATLAS Collaboration, `arXiv:1407.3935`.
[36] ATLAS Collaboration, `arXiv:1406.0076`.
[37] ATLAS Collaboration, ATLAS-CONF-2014-046, `https://cds.cern.ch/record/1741020`.
[38] ATLAS Collaboration, Eur.Phys.J. C72 (2012) 1844.
[39] ATLAS Collaboration, Eur.Phys.J. C70 (2010) 823–874.
[40] S. Agostinelli, et al., Nucl.Instrum.Meth. A506 (2003) 250–303.
[41] G. Bozzi, B. Jaeger, C. Oleari, D. Zeppenfeld, Phys.Rev. D75 (2007) 073004.
[42] F. Campanario, C. Englert, S. Kallweit, M. Spannowsky, D. Zeppenfeld, JHEP 1007 (2010) 076.
[43] J. Alwall, M. Herquet, F. Maltoni, O. Mattelaer, T. Stelzer, JHEP 1106 (2011) 128.
[44] M. L. Mangano, M. Moretti, F. Piccinini, R. Pittau, A. D. Polosa, JHEP 0307 (2003) 001.
[45] A. Alboteanu, W. Kilian, J. Reuter, JHEP 0811 (2008) 010.
[46] W. Kilian, T. Ohl, J. Reuter, Eur.Phys.J. C71 (2011) 1742.
[47] M. Moretti, T. Ohl, J. Reuter, `arXiv:hep-ph/0102195`.
[48] D. Stump, J. Huston, J. Pumplin, W.-K. Tung, H. Lai, et al., JHEP 0310 (2003) 046.